

Technical note

Machine vision photogrammetry: a technique for measurement of microstructural strain in cortical bone

Daniel P. Nicoletta^{a,*}, Arthur E. Nicholls^a, James Lankford^a, Dwight T. Davy^b

^a*Mechanical and Materials Engineering Division, Southwest Research Institute, 6220 Culebra Road, PO Drawer 28510, San Antonio, TX 78228-0510, USA*

^b*Department of Mechanical and Aerospace Engineering, Case Western Reserve University, Cleveland, OH, USA*

Accepted 20 July 2000

Abstract

Understanding local microstructural deformations and strains in cortical bone may lead to a better understanding of cortical bone damage development, fracture, and remodeling. Traditional experimental techniques for measuring deformation and strain do not allow characterization of these quantities at the microstructural level in cortical bone. This study describes a technique based on digital stereoinaging used to measure the microstructural strain fields in cortical bone. The technique allows the measurement of material surface displacements and strains by comparing images acquired from a specimen at two distinct stress states. The accuracy of the system is investigated by analyzing an undeformed image set; the test image is identical to the reference image but translated by a known pixel amount. An increase in the correlation sub-image train parameter results in an increase in displacement measurement accuracy from 0.049 to 0.012 pixels. Errors in strain calculated from the measured displacement field were between 39 and 564 microstrain depending upon the sub-image train size and applied image displacement. The presence of a microcrack in cortical bone results in local strain at the crack tip reaching 0.030 (30,000 microstrain) and 0.010 (10,000 microstrain) near osteocyte lacunae. It is expected that the use of this technique will allow a greater understanding of bone strength and fracture as well as bone mechanotransduction. © 2000 Elsevier Science Ltd. All rights reserved.

Keywords: Cortical bone; Micromechanics; Microstructure; Strain

1. Introduction

A greater understanding of the relationship between globally applied mechanical loads and local or tissue level strains is beneficial in developing an improved comprehension of the mechanisms underlying bone fracture, damage development, and bone remodeling. For example, it is known that bone microstructure plays a role in bone fracture behavior, including interaction of specific microstructural features such as the cement line with crack propagation (Burr et al., 1988; Advani et al., 1992; Guo et al., 1998, 1995), the dependence of bone density and microstructural orientation on bone fracture (Behiri and Bonfield, 1989; Feng et al., 1995; Norman et al., 1995), and the role of microcracks in bone fracture

behavior (Vashishth et al., 1997). It has also been shown that bone behaves like a brittle microcracking material (Schaffler et al., 1995; Zioupos and Currey, 1994) and that these microcracks, on the order of tens or hundreds of microns in size, may stimulate a bone remodeling response (Martin and Burr, 1982; Mori and Burr, 1993). Strain gages and extensometers are the traditional tools used to characterize strain and deformation in cortical bone. However, due to their relatively large size compared to the scale at which strain and displacement information is desired, alternative methods of measurement are required.

The goal of this study was to investigate the application of a full field deformation and strain measurement system to quantify the local, microstructural and cellular level strains in cortical bone. The accuracy of this technique with respect to digital image correlation parameters is investigated. The technique is then applied to quantify the strain field around a microcrack in cortical bone.

* Corresponding author. Tel.: + 1-210-522-3222; fax: + 1-210-522-5122.

E-mail address: dnicolella@swri.edu (D.P. Nicoletta).

2. Methods

2.1. Digital stereoisaging

Digital stereoisaging is a technique based on photogrammetry that allows the measurement of material surface displacements by comparing images of a specimen taken at two different stress states (Davidson and Lankford, 1983; Lankford and Davidson, 1988, Williams et al., 1980). To use the system, an array of measurement points is digitally superimposed on a micrograph taken of the specimen in the reference state, thereby defining where displacement measurements are to be made. The user defines the measurement grid density by indicating the number of grid columns and rows. The image processing system “trains” on (stores in memory) a small area (the model) based on the unique surface texture surrounding each measurement point in the reference image (Fig. 1). A local search is then performed to find the best matching area in the second (deformed) image. The sizes of the user-defined train and search regions generally depend upon available surface detail and material displacement magnitude. The displacement search procedure is controlled by a normalized image correlation algorithm

$$r(u, v) = \frac{N \sum_i I_i M_i - \left(\sum_i I_i \right) \left(\sum_i M_i \right)}{\sqrt{\left[N \sum_i I_i^2 - \left(\sum_i I_i \right)^2 - N \sum_i M_i^2 - \left(\sum_i M_i \right)^2 \right]}}$$

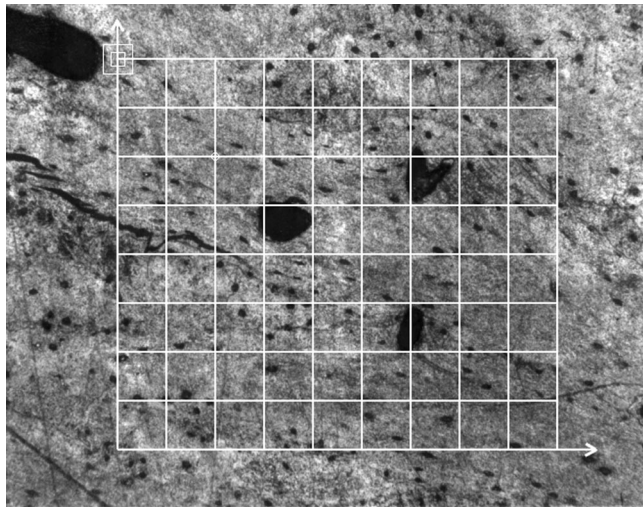


Fig. 1. Digital micrograph of microcracked cortical bone used in unloaded analyses to determine system accuracy. The displacement measurement grid is superimposed on the micrograph and shown at the top-left-corner are graphical representations of the correlation train and search parameters. The inner square represents the sub-image train size and the outer square represents the search size (train = 31 × 31 pixels, search = 63 × 63 pixels). Image resolution = 1312 × 1032 pixels. Original magnification: 200X.

where $r(u, v)$ defines the degree of correlation between the image areas, I is the target (stressed) image region, M is the model (reference) image region, M_i is the model pixel location (x_i, y_i) , I_i is the target pixel location $(u + x_i, v + y_i)$, N is the number of pixels in the model image where i ranges from 1 to N . The trained image area is a square array of pixels (with sides N) around each measurement grid point. A correlation value of $r = 1$ indicates a perfect match, $r = 0$ no correlation, and $r = -1$ is a perfect mismatch (Franke et al., 1991). This algorithm determines the position of the deformed material points with respect to the undeformed image. Rotations are not accounted for with this algorithm; however, the images are first aligned automatically using the image correlation procedure over a large portion of the image to minimize rigid body translations and rotations. All image processing, alignment, and correlation measurement functions are performed with custom software written within the LabView (LabView v.5.0, National Instruments, Austin, TX) programming environment running on a Pentium-based PC. The software system uses the correlation index (r) within the search region to interpolate between pixel locations to calculate fractional pixels and estimate subpixel displacement position. Variations in surface contrast or texture between image sets is also accounted for by adjusting the train and search parameters accordingly. Upon determination of the displacement components for each measurement point, the full, in-plane, two-dimensional strain tensor is calculated by smoothing and numerically differentiating the displacement field (Williams et al., 1980).

2.2. System precision and accuracy

To determine the accuracy and precision of the displacement mapping technique, an analysis was performed using image pairs consisting of identical images; one image was used as the reference image, the second, identical image, was used as the test image. The reference image was digitized using a digital camera (Kodak Mega-Plus Digital Camera, Model 1.41, Eastman Kodak Co., Rochester, NY) at a pixel resolution of 1312 × 1032. The test image was generated by making a copy of the reference image and digitally translating the image in the horizontal direction by a known pixel amount (0, 1, 5, and 10 pixel translation), creating a rigid body displacement. The displacements were measured over a 9 × 10 measurement grid using increasing train areas of 19 × 19 pixels, 31 × 31 pixels, and 63 × 63 pixels (Fig. 1). From the measured displacement field for each analysis, the resulting strains were determined using a previously described method (Williams et al., 1980). Rigid body displacements result in zero strain; calculated strains are thus a measure of system accuracy.

2.3. Example application: cortical bone microstructural strain measurement

To investigate local tissue level deformations and strains in cortical bone, the strain resulting from a microcrack in stressed cortical bone was investigated. The cortical bone specimen was prepared from a fresh bovine tibial bone; rectangular sections were milled flat and parallel to within ± 0.0254 mm under constant irrigation. After machining, each sample was polished using standard metallurgical polishing techniques to a surface finish of $3\ \mu\text{m}$. The initial crack was created by pre-cracking the flat, edge-notched longitudinally oriented specimen of bovine cortical bone with a razor blade; the razor blade was slowly inserted into the notch until a crack approximately $250\ \mu\text{m}$ in length was created at the notch tip. Specimens were tested at 23°C and kept wet with normal saline. Images of the unloaded, but pre-cracked specimen were taken with a Polaroid camera attached to an inverted metallographic microscope at magnifications of 500X. The razorblade was re-inserted into the specimen resulting in a sub-critical stress intensity factor, thus opening the microcrack, and corresponding images were obtained of the stressed specimen at the same magnifications. The loaded and unloaded images were digitized with the digital camera at a resolution of 1312×1032 pixels. The microstructural strain field was calculated from displacements measured using a local sub-image train size of 63×63 pixels.

3. Results

3.1. Precision and accuracy

Increasing the local sub-image train size resulted in an increase in displacement measurement accuracy (Fig. 2). The maximum error in grid point location for the 90

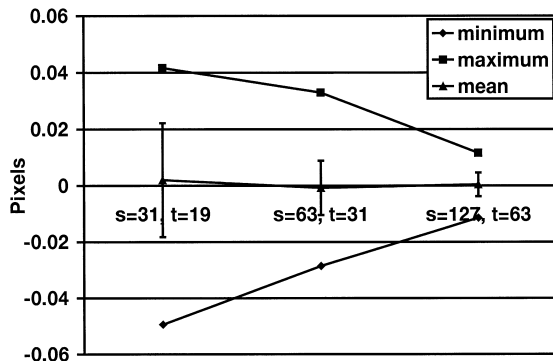


Fig. 2. Effect of correlation train parameter on sub-pixel displacement measurement resolution (s = search, t = train). Shown are the minimum, maximum, and mean error over 90 measurement points. Error bars on mean values indicate one standard deviation.

measurement points used was 0.049 pixels for a train size of 19×19 pixels and 0.012 pixels for a train 63×63 pixels. Increasing the train parameter size also resulted in a reduction of the mean displacement error from 0.002 pixels (standard deviation, $\text{SD} = 0.02$) for the 19×19 pixel train size to 0.0004 pixels ($\text{SD} = 0.004$) for the 63×63 pixel train size. There was minimal effect of the magnitude of applied image displacement on displacement measurement accuracy (Fig. 3). All errors were normally distributed about their means.

The strains in the horizontal direction (ϵ_{xx}) calculated from the measured displacement fields also showed an increase in accuracy with an increase in sub-image train size (Fig. 4). Maximum error in the computed strain was reduced from 564 microstrain using a train size of 19×19 pixels to 133 microstrain using a train size of 63×63 pixels for the 10 pixel displacement case. Increasing applied image displacement resulted in an increase in computed strain (Fig. 4) for all sub-image train sizes. The average computed strain varied from a maximum of 4.52 microstrain ($\text{SD} = 66.58$) for the 10 pixel displacement case using a train size of 31×31 pixels to 0.00 microstrain ($\text{SD} = 16.39$) for the 0 pixel displacement case using a train size of 63×63 pixels. The other strain tensor components showed similar results. All errors were normally distributed about their means.

3.2. Microcrack specimen

The presence of a microcrack in cortical bone results in the local strain at the crack tip reaching 0.030 (30,000 microstrain). A plot of the effective strain (Davidson and McClung, 1997)

$$\epsilon_{\text{eff}} = \frac{2}{\sqrt{3}}(\epsilon_1^2 + \epsilon_2^2 + \epsilon_1 \epsilon_2)^{1/2}$$

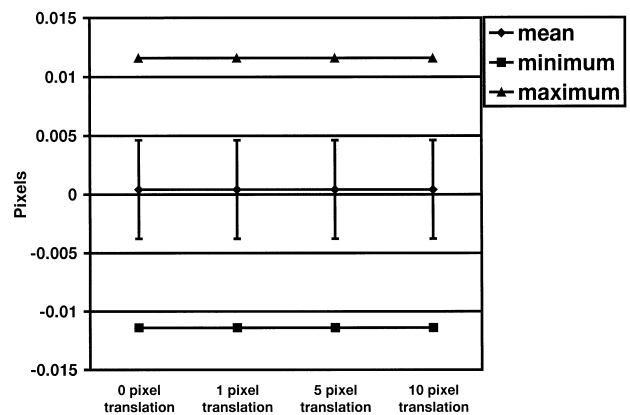


Fig. 3. Displacement magnitude had little effect on sub-pixel measurement accuracy. As the magnitude of applied displacement increased, the maximum, minimum, and mean measurement error remained constant. Data shown is for the 63×63 pixel correlation train size. The other train sizes showed identical results. Error bars on mean values indicate 1 SD.

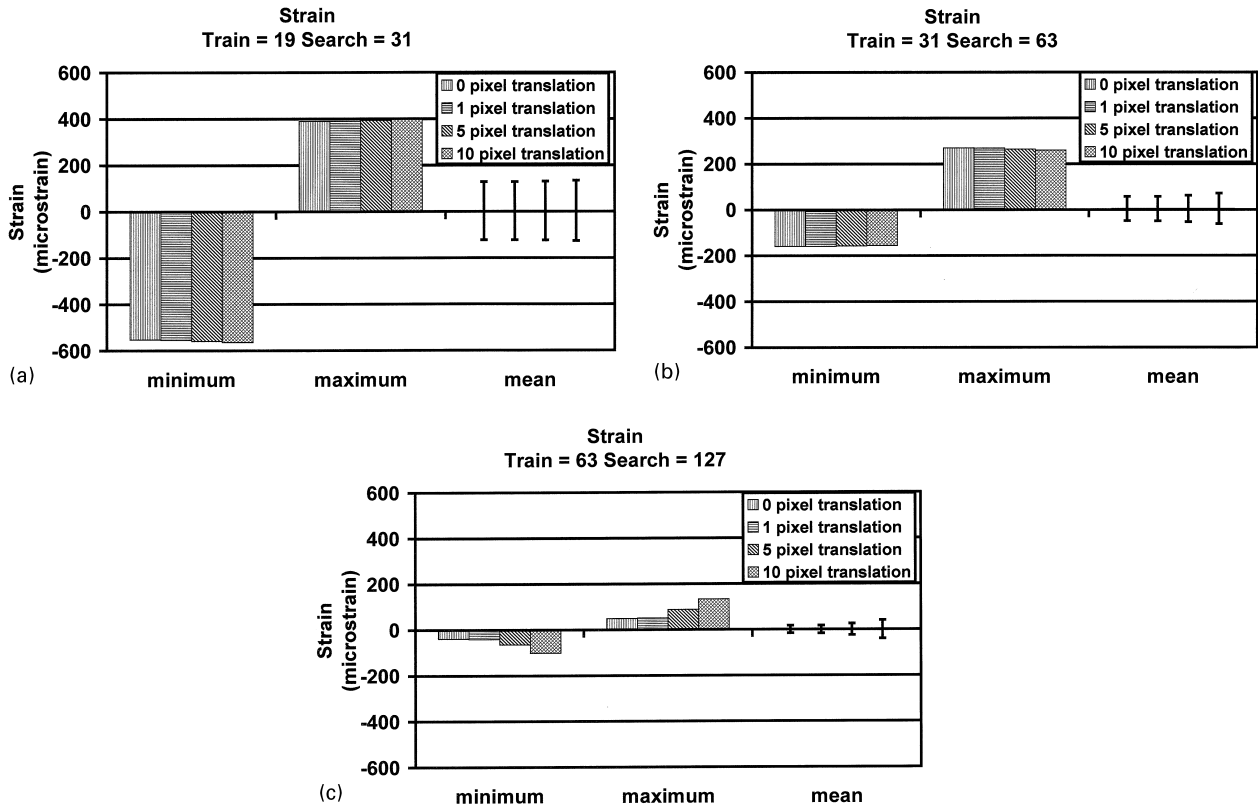


Fig. 4. Increasing the correlation train parameter resulted in an increase in strain accuracy. Maximum strain measurement error ranged from 564 microstrain corresponding to a train size of 19×19 pixels to 133 microstrain corresponding to a train size of 63×63 pixels. An increase in the applied displacement magnitude resulted in an increase in strain measurement error. Error bars on mean values indicate one standard deviation. All strain tensor values showed similar results. A: train = 19, search = 31; B: train = 31, search = 63; C: train = 63, search = 127.

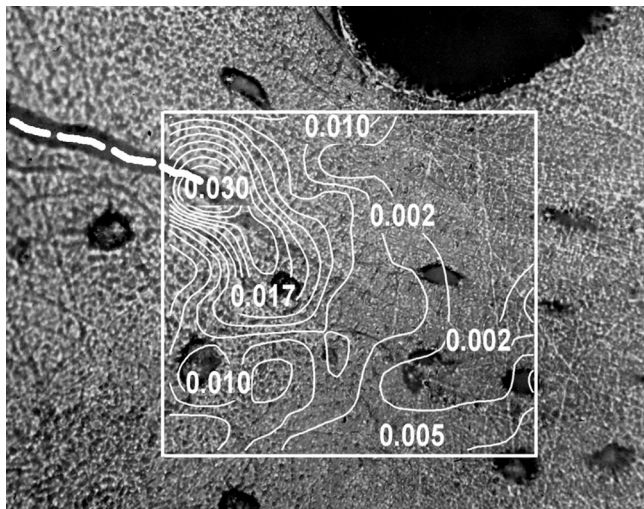


Fig. 5. Digital micrograph of bone surface taken at 500X magnification. Superimposed on the micrograph is the resulting effective strain field. The effect of microstructural features such as osteocyte lacunae (arrows) on the strain field is evident. The dashed line shows the location of the microcrack tip. Local strain reaches 30,000 microstrain at the crack tip and 10,000 microstrain near an osteocyte lacuna.

(where ϵ_1 and ϵ_2 are the principal strains) over this area reveals a region of high tissue strains present at the crack tip (Fig. 5). The measurement grid spacing used, $11 \mu\text{m}$, captures the complexity of the strain field at this microstructural level revealing the effects of microstructural features such as osteocyte lacunae. Local strain concentrations on the order of 0.010 strain (10,000 microstrain) are associated with osteocyte lacunae (Fig. 5) as a local peak in the strain field.

4. Discussion

Understanding local microstructural deformations and strains in cortical bone may lead to a better understanding of cortical bone damage development, fracture, and remodeling. An image correlation technique, based on digital stereo photogrammetry, used to quantify the microstructural deformation and strain fields in cortical bone has been presented. The random nature of the bone surface texture is used to track the displacements of unique material points between distinct stress states, with subsequent measurement accuracy dependent on the

level of image detail present. The correlation sub-image train parameter determines the accuracy of the procedure, which has been shown to be less than 0.02 pixels. The overall performance of this system is similar to other two-dimensional image correlation systems (Lyons et al., 1996).

The results presented here, obtained from the analyses of undeformed image sets, represent the baseline accuracy that can be expected using this image-based displacement measuring system. As the material deforms, additional error will be introduced due to the local deformation of the sub-image train area from the undeformed to the deformed state. Additional error can result from poor surface texture, which will result in incorrect correlation matches, hence erroneous displacement measurements. Furthermore, some image sets may contain a heterogeneous level of detail resulting in regions in which the correlation directed search performs poorly (low surface detail) as compared to other regions within the same image (high surface detail). This can be compensated for by selectively adjusting the correlation parameters for specific measurement points that return low correlation values and re-analyzing those points. However, some care must be taken when selecting correlation parameters. Although a larger train size increases the accuracy of the displacement measurements, larger train areas also may result in the averaging of local strain fields in which high strain gradients exist. Therefore, when choosing the correlation parameters, the expected strain gradients and the level of image textural detail should be taken into consideration. As such, the optimal correlation parameters must be determined for each image set and analysis.

Local strain fields in the microcracked specimen were shown to reach over 30,000 microstrain within a local area ahead of the microcrack. As shown by Vashishth et al. (1997), microcracks form in a “process zone” ahead of the crack tip as the crack propagates through the bone specimen. These microcracks are a consequence of local tissue failure caused by the localized, intense strain concentration at the crack tip. This process zone is highly complex, and is influenced by the bone microstructure; multiple strain peaks are present not only at the crack tip, but adjacent to the osteocyte lacuna as well (Fig. 5). High strains around osteocyte lacunae associated with microcracks may contribute to the observed remodeling response to bone microdamage (Mori and Burr, 1993; Burr et al., 1985).

Acknowledgements

The authors would like to thank Mr. Jim Spencer and Mr. Don Moravits for their technical assistance with the

DISMAP system. This work was supported by NIH Grant AR43785 and the Southwest Research Institute Advisory Committee for Research under Project R9105.

References

- Advani, S.H., Lee, T.-S., Martin, R.B., 1992. Analysis of crack arrest by cement lines in osteonal bone. *Advances in Bioengineering. ASME BED* 3, 57–58.
- Behiri, J.C., Bonfield, W., 1989. Orientation dependence of the fracture mechanics of cortical bone. *Journal of Biomechanics* 22, 863–872.
- Burr, D.B., Martin, R.B., Schaffler, M.B., Radin, E.L., 1985. Bone remodeling in response to in vivo fatigue microdamage. *Journal of Biomechanics* 18, 189–200.
- Burr, D.B., Schaffler, M.B., Frederickson, R.G., 1988. Composition of the cement line and its possible mechanical role as a local interface in human compact bone. *Journal of Biomechanics* 21, 939–945.
- Davidson, D.L., Lankford, J., 1983. The effect of water vapor on fatigue crack tip mechanics in 7075-T651 aluminum alloy. *Fatigue of Engineering Materials and Structures* 23, 241–256.
- Davidson, D.L., McClung, R.C., 1997. Local constraint near fatigue cracks in alloys and particulate composites. *International Journal of Fracture* 84, 81–98.
- Feng, Z.D., Rho, J.Y., Ziv, I., 1995. Mode II fracture toughness of cortical bone — a comparison of longitudinal and transverse crack propagation. *Advances in Bioengineering. ASME BED* 29, 419–420.
- Franke, E.A., Wenzel, D.L., Davidson, D.L., 1991. Measurement of microdisplacements by machine vision photogrammetry (DISMAP). *Review of Scientific Instruments* 62, 1270–1279.
- Guo, X.E., Liang, L.C., Goldstein, S.A., 1998. Micromechanics of osteonal cortical bone fracture. *ASME Transactions Journal of Biomechanical Engineering* 120, 112–117.
- Guo, X.E., He, M.Y., Goldstein, S.A., 1995. Understanding cement line interface in bone tissue: a linear fracture mechanics approach. *Advances in Bioengineering. ASME BED* 29, 303–304.
- Lankford, J., Davidson, D.L., 1988. The micromechanisms of small fatigue crack growth and the influence of metallurgical structure. In: E.A. Starke, Ritchie, R.O. (Eds.), *Fatigue 87. Engineering Materials Advisory Services, Ltd, Cradley Heath, UK*, pp. 1769.
- Lyons, J.S., Liu, J., Sutton, M.A., 1996. High-temperature deformation measurements using digital-image correlation. *Experimental Mechanics* 36, 64–70.
- Martin, R.B., Burr, D.B., 1982. A hypothetical mechanism for the stimulation of osteonal remodelling by fatigue damage. *Journal of Biomechanics* 15, 137–139.
- Mori, S., Burr, D.B., 1993. Increased intracortical remodelling following fatigue damage. *Bone* 14, 103–109.
- Norman, T.L., Vashishth, D., Burr, D.B., 1995. Fracture toughness of human bone under tension. *Journal of Biomechanics* 28, 309–320.
- Schaffler, M.B., Choi, K., Milgrom, C., 1995. Aging and matrix microdamage accumulation in human compact bone. *Bone* 17, 521–525.
- Vashishth, D., Behiri, J.C., Bonfield, W., 1997. Crack growth resistance in cortical bone: Concept of microcrack toughening. *Journal of Biomechanics* 30, 763–769.
- Williams, D.R., Davidson, D.L., Lankford, J., 1980. Fatigue-Crack-Tip Plastic Strains by the Stereoimaging Technique. *Experimental Mechanics* 20, 134–139.
- Ziopoulos, P., Currey, J.D., 1994. Extent of microcracking and the morphology of microcracks in damaged bone. *Journal of Materials Science* 29, 978–986.